J Opt
https://doi.org/10.1007/s12596-024-02204-2

RESEARCH ARTICLE

Tuning the optical absorption and band gab of hydrogel methylcellulose loaded using hybrid Fe_3O_4@GO nanomaterials for optoelectronic and antibacterial activity

Rafah Mahdi Ahmed[1,2] · **Ehssan Al-Bermany**[1]

Received: 1 June 2024 / Accepted: 24 August 2024
© The Author(s), under exclusive licence to The Optical Society of India 2024

Abstract Hydrogel polymer nanocomposites are exciting materials with specific structural characteristics that absorb and maintain a large amount of biological fluid or water. This investigation focused on comparing reinforced methylcellulose (MC) polymer with individual synthesis of graphene oxide (GO) nanosheets or iron oxide (Fe_3O_4) nanoparticles or combined between them as hybrid nanomaterials. An advanced solution-acoustic-sonication procedure was applied with several characteristics to examine the hydrogel-nanocomposites. Remarkable strong physical interfacial interaction between the nanomaterials with MC resulted in shifting in infrared Fourier transform spectroscopy spectra without effect on the MC semicrystalline behavior. Delicate homogeneous, rough surfaces and nanoclusters were revealed using optical and field emission electron microscopy. The absorption of electron transition at 200 nm was improved by up to 21% after incorporating hybrid nanomaterials. The optical energy gap notably enhanced the semiconductor area from 4.79 to 4.0 eV for the allowed indirect transitions and 4.05–3.05 eV for forbidden indirect transitions. GO@Fe_3O_4 hybrid nanomaterials revealed an interesting inhibition zone of the antibiotic, remarkably improving from 6 mm up to 26 and 25 mm for *Staphylococcus aureus* and *Escherichia coli*, respectively, mm compared to reinforced with one nanocomposite. These results of a combination of magnetic, electrical, and surface properties make them ideal for various applications ranging from optoelectronic devices and environmental remediation to advanced biomedical technologies.

Keywords GO · Fe_3O_4 · MC · Nanocomposites · Optical · Antibacterial

Introduction

Hydrogel polymers are a specific kind of polymers that form a 3D network structure [1]. These polymers have specific structural characteristics that allow them to absorb and maintain much biological fluid. They have wide applications in a variety of fields through their exclusive properties, including biocompatibility, adjusted mechanical properties, and high water content [2]. Several hydrogel polymers are stimulus-responsive to external factors such as light, temperature, pH, or electric fields. Hydrogels can be responsive in a reversible way wherein they can change their size, shape, or mechanical properties according to the environment [3]. Thus, these synthetic polymeric hydrogels are increasingly being proposed for numerous applications, such as drug delivery [4], sensing [5], etc. The formulation and processing of hydrogel polymers can be very sophisticated, and the production of these polymers can require a high degree of control over many parameters, including polymer composition, crosslinking density, and manufacturing processes. This will significantly increase the complexity of repeatable results and production scalability [6].

Some hydrogel polymers do not possess good mechanical properties: low tensile strength, fragility, etc., which may hinder their implementation in situations with high loads or such applications as building tissue engineering scaffolds [7]. Hydrogel polymers exhibit a high absorption capacity and might expand significantly when exposed to water or

✉ Ehssan Al-Bermany
ehssan@uobabylon.edu.iq

[1] Department of Physics, College of Education for Pure Sciences, University of Babylon, Babylon, Iraq

[2] Educational Directorate of Babylon, Ministry of Education, Babylon, Iraq

Published online: 03 September 2024

biological fluids. However, swelling might occur excessively and lead to mechanical inhomogeneity, structural insufficiency, or bursting. Moreover, hydrogels may lose water and become dehydrated in dry conditions [8]. In comparison, the sol state is characterized by the dispersion of polymer chains, which are surrounded and dissolved by the solvent. In this state, the material exhibits fluid-like or liquid-like behavior. In this condition, the polymer chains are not linked to create a stiff structure, which enables the material to move quickly [9]. Solutions commonly display reduced viscosity and possess a more fluidic nature [10].

Since the behavior of the hydrogel polymers exposed to the solvent can vary, depending on their natural categories, the swelling or dissolution of the hydrogels in contact with the solvent may occur. Specifically, swelling is a process where the solvent can penetrate the hydrogel network, whereas dissolution describes the complete disintegration of the former structure to develop a consistent solution [11]. Therefore, one can manipulate the following factors, including ionic strength, pH, temperature, and solvent composition, to regulate the transformation of hydrogel to sol polymer [12]. These factors can affect the chemically controlled swelling pattern, dissolving kinetics, and mechanical behavior of the formed sol polymer. Also, hydrogen peroxide enzymes can disrupt or destroy the crosslinks [10].

Methylcellulose (MC) is a highly synthetic hydrogel polymer with a molecular formula ($C_{20}H_{38}O_{11}$), consisting of many glucose molecule links. Methylcellulose (MC) serves as a stabilizer, thickener, and canning agent for both foodstuffs and cosmetics [13]. The substitution degree is determined by calculating the mean number of hydroxyl groups replaced with other atoms or groups per glucose molecule. Methyl cellulose is a colorless powder soluble in cold water but not in hot water. When dissolved in cold water, it forms a transparent and thick solution or gel [14]. It is marketed under many brand names as a remedy for constipation. It is available under various trade names as a treatment for constipation. MC is indigestible and non-toxic [15]. The large intestine does not absorb methylcellulose, attracting large amounts of water to the colon. It is used as an emulsifying and suspending agent in medicines and the chemical industry [16].

Adding a small number of nanomaterials leads to significantly improving many properties of hydrogel polymer without losing the light weight of the polymer matrix and reducing the weaknesses of the polymers [17, 18]. The polymer matrix demonstrates the presence of compatibility, homogeneity, interaction, and fine dispersion of the nanofillers [19]. The most challenging aspect of nanocomposites is the inherent difficulty in integrating the nanoparticles or the incompatibility that causes the nanomaterials to aggregate [20]. Enhancing the characteristics of nanocomposites can be a solution to address these significant obstacles [21].

Graphene is a carbon atom that has caused significant transformations in both academia and industry [22]. Graphene is one of the most promising nanofillers with a hexagonal structure. Graphene oxide (GO) is a graphene derivative that is a single carbon layer with a 2D dimensional and reduced graphene oxide (rGO). It has numerous active groups (oxygen groups) on its surfaces [23]. These materials are crucial components in the production of various graphene-based nanomaterials [24]. Graphene oxide (GO) is a carbon-based material with a flat, two-dimensional shape and a hexagonal crystalline structure, like a honeycomb or chicken wire [25]. The presence of oxygen in it hinders its ability to conduct electricity effectively. It is a material that has had a transformative impact on the technology field. It consists of atoms with a single layer. By reducing the size of iron particles to the nanoscale scale, it is possible to generate smaller bands and increase the effective band gap [26]. Crystalline graphene oxide is essential for producing semiconductors and microelectronic devices in modern electronics [27]. Graphene is highly suitable for photothermal applications because of its substantial optical absorption in the near-infrared bands and its exceptional and distinctive structure [28, 29].

Fe_3O_4 nanoparticles are promising nanomaterials due to their compatibility with magnetic materials, and iron oxide biocompatibility is the main driving force of significant research energies. Its two-dimensional structure, the color of white granules, odorless and tasteless [30]. The melting point of Fe_3O_4 is 1591 degrees Celsius, and its solubility in water produces a transparent to opalescent solution [31]. It is stable at room temperature, and when heated, it decomposes, emitting acrid smoke and irritating fumes. It is commonly used as an all-purpose food ingredient in biopharmaceuticals and animal feed. It is safe when used according to good manufacturing and nutritional practices [32]. Due to the properties of ferromagnetism, semi-metallicity, and biocompatibility, Fe_3O_4 can be successfully applied in materials science, chemistry, physics, and so forth [22]. The production of Fe_3O_4 has taken a wide range of forms and sizes, and its properties have been thoroughly studied in these fields due to the importance of the performance of Fe_3O_4. At the same time, the number of applications and methods for its structure and the changes in its function have been gradually developed [33, 34]. Several procedures have been applied to synthesize and control the structure or properties of Fe_3O_4 nanoparticles in various characteristics, dimensions, etc., for the crucial influence of Fe_3O_4 in different applications, for instance, medical, electronic, environmental, energy, and so on [35, 36]. The incompatibility of Fe_3O_4 in the polymer matrix is the main challenge facing the researchers in overcoming this problem using different strategies. For instance, Fe_3O_4 has been functionalized or combined with

other nanomaterials, oxides, metals, and other materials to improve its compatibility in the polymer matrix [37, 38].

In recent times, scientists and engineers have endeavored to amalgamate several nanomaterials to achieve distinctive characteristics in nanocomposites [37, 39]. The combination of two nanomaterials, graphene oxide (GO) and iron oxide (Fe_3O_4), is achieved [40–42]. There are two prevalent and widely used approaches for deploying the structure and characteristics of materials for diverse purposes [39, 43].

HS Rajab, MFH, Abdel Qader, (2013) [14] starch was mixed with methylcellulose (MC) to prepare blends using casting technology. The samples exhibited notable alterations in the combination samples' IR spectra, suggesting intermolecular interactions between the starches (MC). The UV–Vis analysis demonstrated a reduction in the optical band gap values as the MC content in the mixed samples increased [44]. Each sample of the poly combination had a singular glass transition temperature. The thermogravimetric analysis data assessed the kinetic thermodynamic parameters, including activation energy, enthalpy, entropy, and Gibbs free energy. According to Atta A. and Hamid M. [45], MC, PANI, and AgNPs were successfully synthesized via casting technique to increase the photovoltaic role. The obtained results assured that the difference in energy bandgap of the MC/PANI/Ag NPs is lower than that of the pure film for MC. Additionally, the Ag NPs raised the predicted carbon mass. The intake of Ag NPs, in addition to others and PANI, enhanced the optical attributes of the MC polymer, forming a modernly developed component suitable for energy conversion systems, cells, solar, biosensors, and nonlinear optical functions. The study conducted by Sohouli E. et al. [46] reported a high-performance electrochemical bioassay system (GCE) design using a modified glassy carbon electrode to produce MC-GO-Fe_3O nanocomposites-hydrogel. A modified glassy carbon electrode. Differential pulse voltammetry (DPV) and cyclic voltammetry (CV) techniques were used to analyze the electrooxidation of uric acid (UA) that GCE modified. A developed electrode was investigated to measure UA, and it was reported that UA concentration presented a linear dependence. In addition, to detect a linear amplitude of 0.5–140 µM with a detection limit of 0.17 µM. The finding presented that the produced system gives an accurate, precise assay pathway of uric acid in the sample. Yin S. and Zhang T.(2023) [42] reported the successful fabrication of GO@ Fe_3O_4 2D nanocomposites, which are magnetically oriented. Reaction conditions and material ratios significantly impacted coating Fe_3O_4. The strength and direction of the magnetic field, as well as the solid composition of the GO@Fe_3O_4 sol, can control the features listed above. The findings indicate that GO@Fe_3O_4 nanocomposites, which are magnetically orientated in two dimensions, have promise for use in photonic switches, gas barriers, and display devices.

The high absorption ability of GO, coupled with the remarkable magnetic properties of Fe_3O_4, facilitates the creation of exceptional materials for developing sensors capable of detecting magnetic or electrochemical fields, environmental contaminants, and biological and dental substances [47]. Nanomaterials possess a large surface area, enabling them to identify heavy metals, glucose, and other analytes effectively [48]. Furthermore, the nanocomposite's antibacterial activities increase oxidative stress, further amplified by many functional groups [47]. Fe_2O_4 bacterial membranes may be effectively targeted and destroyed by this substance, making it highly promising for applications in coatings, medical devices, fabrics, and surfaces [49, 50]. The wide range of applications stems from the distinctive amalgamation of GO's high surface area and electrical properties with Fe_3O_4's magnetic and catalytic functions [51]. Furthermore, this study specifically examined the potential of optical characteristics to not only attract attention for their characterizations but also their ability to activity against the bacteria by containing reactive oxygen groups, which are species with oxidative properties, and by addressing the stress induced by reactive oxygen radicals (ROS) [52]. The radicals mentioned are superoxide dismutase, hydroxyl radicals (–OH), and (2–0) radicals (H_2O_2) [53]. These components are involved in the chemical process of oxygen radicals, causing damage to the DNA and proteins of bacteria [54].

Nanoparticles should establish communication with bacterial cells to provide an effective antibacterial impact. Electrostatic attraction [55], van der Waals forces [56], receptor-ligand interactions [57], and hydrophobic interactions [58]. Nanoparticles penetrate the bacterial membrane and accumulate along the metabolic pathway, causing changes in the structure and functionality of the cell membrane. The nanoparticles (NPs) subsequently engage with enzymes, DNA, ribosomes, and lysosomes within the bacterial cell, consequential in oxidative stress, diverse alterations, modifications in cell membrane permeability, disturbances in electrolyte balance, gene expression changes, deactivation of proteins, and inhibition of enzymes [59]. The primary mechanism of nanoparticles exert toxicity on bacteria is by inflicting damage to the cell membrane. In addition to causing damage to the cell membrane, the production of reactive oxygen species, disruption of metal/metal ion balance, malfunctioning of proteins and enzymes, and genotoxicity are also observed [59].

There is a limitation of research on the combination of MC polymer with GO or Fe_2O_4, and a lack of studies comparing and complaining these two nanomaterials with MC in one investigation, to the best of our knowledge. However, despite previous investigations on using GO or/ and Fe_2O_3 mixing with another polymer, this is the first analysis focusing on the optical properties and their relationship with the antibacterial inhibitory zone [60]. The variations

in the surface structure, porosity, or layer arrangement of GO and Fe_2O_4 nanoparticles inside the matrix might enhance interactions, hence improving attributes such as adsorption, catalytic activity, or antibacterial efficacy [61]. Furthermore, implementing novel or enhanced techniques results in variations in structural relationship characteristics, distribution, and performance, affecting overall effectiveness [62]. The precise combination of MC, GO, and Fe_2O_4, along with adding extra functional groups or doping elements, can potentially improve features such as magnetism, conductivity, or mechanical strength compared to current nanocomposites [63]. The MC/GO-Fe_2O_4 nanocomposite can potentially improve optical absorption or electrical conductivity, increasing its suitability for applications such as sensors, energy storage, or environmental remediation [64]. This novel nanocomposite can be customized for specific purposes, such as enhancing photocatalytic activity [65], developing drug delivery systems, or improving antimicrobial properties, distinguishing it from previously reported composites [66]

Despite several research in this field, limited studies focus on the impact of GO, Fe_3O_4, or GO@Fe_3O_4 on MC hydrogel polymer that could notably improve in industrial and medical applications. To better understand and reduce the knowledge gap about these exciting materials in this area. Several samples were made into three groups: first, MC was reinforced with GO nanosheets; second, MC-GO nanosheets nanocomposite; and third, MC/GO-Fe_3O_4 nanocomposite was fabricated in the shape of a sol–gel procedure for the first time. Applying several characterizations such as FTIR, XRD, FESEM, UV–Vis, and antibacterial activity.

Materials

Methylcellulose (MC) with the molecular formula $(C_3H_5NO)_n$ in white color and crystal-granular appearance, physical form is a powder with assay (90–99%), ash as (NA_2SO_4): 1.5% Max, methoxyl: 25–33%, moisture as packed: 10.0% Max, 2% viscosity, (20 °C): 4000 mPas, pH: 5.0–8.0, and gelation temperature: 50–55 °C, supplied from Vibration Chemicals, the UK. Fe_3O_4 spherical nanoparticles with 20–30 nm and purity up to 98 + with trace metals basis supplied by Sky Spring Nano Materials, Algeria. Our group synthesized graphene oxide (GO) following the procedure with complete characterization provided in the previous publication [19].

Methods

MC powder was first dissolved in distilled water (DW) for 6 h, with a hydrogel consistency. Secondly, 5% of Fe_3O_4 was dispersed in DW for 2 days and then loaded to hydrogel MC polymer to prepare MC/Fe_3O_4 nanocomposites (R1). Thirdly, 5% of synthesis GO was dispersed in DW for a week and then added to hydrogel MC polymer to prepare MC/GO nanocomposites (R2). Both samples R_1 and R_2 were sonicated in a sonication bath through the mixing procedure for 30 min. Fourthly, 2.5% for each nanomaterial for Fe_3O_4 and synthesis GO were dispersed together in distilled water (DW) for two days and then added to hydrogel MC polymer to prepare MC/Fe_3O_4@GO nanocomposites, named (R_3). The preparation of ternary MC/Fe_3O_4@GO hybrid nanocomposites (R_3) involved using sonication in a sonication bath for an average of 30 min, as shown in Table 1. Samples were placed in the plastic Petrie dish for specific tests. Figure 1 revealed photographic images during the preparation of hydrogel MC-mixing with DW, MC-stope mixing as sol–gel MC, GO@Fe_3O_4-DW nanomaterials, GO@Fe_3O_4-DW top view after left for a day, R_1, R_2, and R_3after loaded nanomaterials as sol–gel nanocomposites and R_1, R_2, and R3 after loaded nanomaterials as dried films under air for 4 days, with thicknesses between 150–170 µm of final dried films.

Antibacterial activity

4–5 isolated colonies were designated from a 24-h culture and diluted. lThe Mueller Hinton broth's turbidity is 0.5 Mc Farland's standard. The agar disk diffusion method was utilized to make the antibacterial susceptibility test of synthesized nanocomposites. Using an agar well diffusion procedure, this examination included testing against two bacterial strains, negative and positive Gram [67, 68]. It is implemented at the Phi Nanoscience Center (PNSC), Baghdad, Iraq. Roughly 20 ml of Muller–Hinton agar (MH) were aseptically distributed into sterile Petri dishes. A sterile wire loop was used to get bacterial strains from their respective stock cultures [69]. Following the organism's cultivation, six mm wells were synthesized on the agar plates using a sterile tip. The same ratio of samples was loaded. At 37 °C, it was left to incubate overnight; the inhibition zone average diameter was then designed [70, 71].

Table 1 Mixing concentrations of prepared hydrogel samples

Sample Code	Concentration Wt. %		
	MC	GO	Fe_3O_4
MC	100	0	0
R_1	99.95	0.05	0
R_2	99.95	0	0.05
R_3	99.95	0.025	0.025

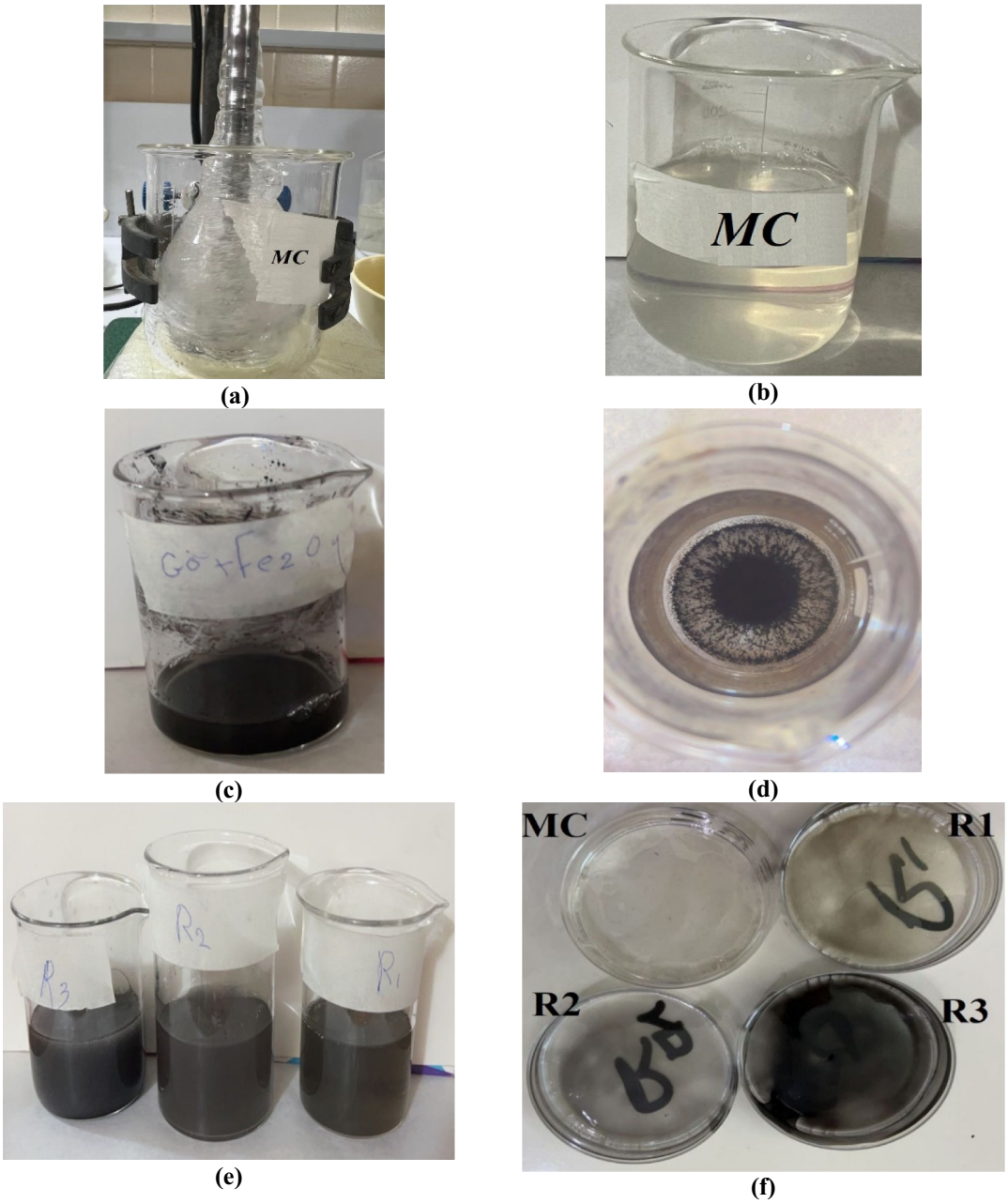

Fig. 1 Photographic images during the fabrication procedure of **a** hydrogel MC-mixing with DW, **b** MC-stope mixing as sol–gel samples, **c** GO@Fe_3O_4-DW, **d** GO@Fe_3O_4-DW top view, **e** R1, R2, and R3 as sol–gel samples and **f** R1, R2 and R3 as dried films

Characterization

Table 2 provides an overview of all the characterizations utilized in this examination.

Results and discussion

In Fig. 2, MC revealed functional groups at 3450 cm^{-1} correlated to (O–H), the hydroxyl stretching vibration group; the peaks at 2927 and 2832 cm^{-1} qualified to the (C–H), asymmetric vibration; the functional at 1650 cm^{-1} linked to C = C; peaks at 1460 and 1372 cm^{-1} allocated to C–O and C–H vibration, respectively, large shoulder group at 1054 cm^{-1} ascribed to stretching C–O–C mode, which also reported related to C–O stretch as a hydro glucose ring of C–O–H; and peak at 0942 cm^{-1} linked to O-CH_3 functional groups or hydrophilicity [14].

The contribution of GO, Fe_3O_4, and GO@ Fe_3O_4 revealed shifting in several peaks from 3450 to 3445, 2927 to 2915,

Table 2 Summarized the name, model, details, and manufacturing of the characters utilized

Device	Model	Details	Manufacturing and State
FTIR	Spectrum IR-10.62	500–4000 cm^{-1}	Perkin Elmer, USA
X-ray	AERIS	5–80°	PANalytical, Netherland
FESEM	INSPEC	F50	FEl, Netherland
UV	UV–2100	190–1100 nm	Shimadzu, Japan
Digital calipers	RS PRO Electronic Digital Vernier Caliper with LCD Display	Give you about .01 mm/.0005″ resolution and accuracy 0.03 mm	RS Components Philippines

2832 to 2843, 1650 to 1644 and 1054 to 1048 cm^{-1}. This shifting exposed the bonding interfacial interactions in H–H-bonding could be between the GO and Fe_3O_4 functional groups with MC, the presence of hydrogen bonding contact between the filler and polymer matrices in various composite systems is further confirmed by the displacement of the O–H, C–H, and C–O stretching band (Fig. 2). These results matched other literature [14, 43, 46]. Moreover, GO@Fe_3O_4 nanomaterials presented their contribution to the MC matrix. In contrast, some GO peaks overlapped with MC bands, and others linked with MC peaks led to shifting such as (O–H), C = C, C–H, and C–O. Also, this behavior was continuous with the adding Fe_3O_4 nanomaterials; in addition, there is a peak singe at around 569 cm^{-1}, which is associated with (Fe–O) presented in both R2 and R3, confirming the existence of Fe_3O_4 [46].

Figure 3 observes the diffraction peak of MC spectra, which presents a crystalline seater and some amorphous. A broad peak presented 2θ = 20.66°, a crystal phase structure in agreement with the literature [72]. The MC/GO (R1) was presented with peaks at 10.70° and 42.10°, which are typical GO features [73], where the GO contribution revealed a shift to MC peaks from 20.66° to 20.55°. Also, the MC peak with the contribution of Fe_3O_4 exhibited very similar to that of the pristine of (R1) but with another shifting from 20.66° to 20.09° in the (R2). Whereas the GO-Fe_3O_4 in the (R3) revealed shifting in the MC peak to 21.06° compared with the MC sample, in addition, GO presented at 10.70° and 43.80°, whereas the Fe_3O_4 peaks at 19.19°, 30.80°, 36.36°, 57.80° and 63.38°agreement with compared with the magnetite (JCPDS no.- 96–900–7645) literature [74]. These findings suggest that the GO sheets maintain their exfoliation within the polymer matrix without clumping together or aggregating, indicating high phase purity of cubic Fe_3O_4. Moreover, R3 represented shifting to a higher value from 20.70° to 21.10° compared with the MC polymer; this shifting is related to the contribution of GO-Fe_3O_4 hybrid nanomaterials. Bragg's law calculates the crystal lattice from the Eq. (1) [75].

$$2d \sin\theta = n\lambda \quad (1)$$

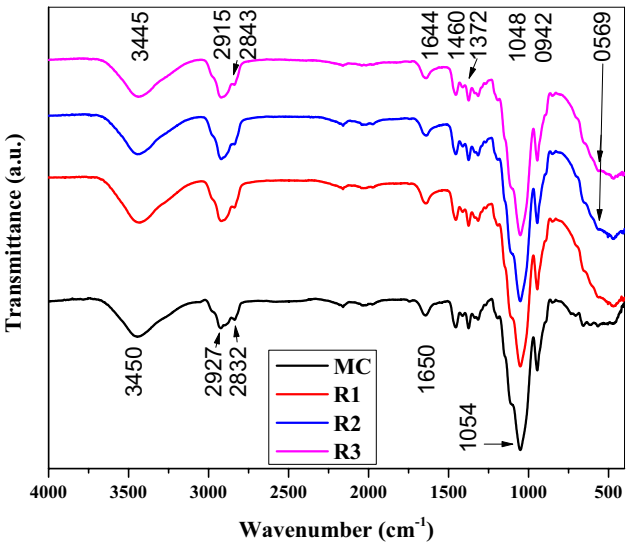

Fig. 2 FTIR spectrum for samples with the wavelength

(θ) is Bragg diffraction angle (degree), (λ) is wavelength coincident of X-ray beam (Å), (d) is distance, and (*n*) is

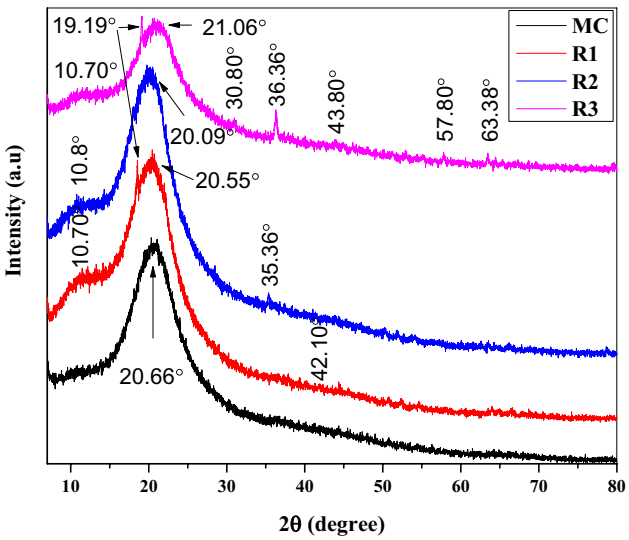

Fig. 3 XRD patterns with diffraction angle for sample

diffraction rating. The size of the crystal (D nm) was calculated using the Scherrer formula (2) [76].

$$D = k\lambda/\beta \cos(\theta) \quad (2)$$

B means the complete range at half the highest point (FWHM), and k equals 0.9. The lattice strain (ε) can be considered by Eq. (2) [76].

$$\varepsilon = \beta/4 \tan(\theta) \quad (3)$$

From the value of lattice strain in Table 3 and Fig. 3, the samples R1 and R2 shifted to higher values than means a compressive strain (negative strain) and uniform deformation throughout the crystal lattice as uniform strain (Homogeneous Strain). Even R3 has a higher lattice strain value than MC, but it is a less homogeneous strain than R1 and R2 because it combines two different nanomaterials. Interestingly, the small shifting in the R3 due to the contributions of hybrid nanomaterials refers to a uniform shift in peak positions without significant broadening, suggesting that the entire crystal lattice is uniformly stretched or compressed, altering the lattice parameters across the whole material [77]. Table 3 summarizes the diffraction angle (2θ), interlayer displacement (d), crystallite size (D), typically FWHM (β), and Lattice Strain of samples.

FESEM images of the MC film and nanocomposite films are shown in Fig. 4. The MC exposed a smooth fracture surface with fewer savages that could be related to the air poles after drying the samples. R_1 samples showed changes in the surface fractures of the samples that become dense and rough with clear GO flakes presented on the surface of the samples in both images of the R1 sample, with the nanosize of GO flakes. At the same time, R_2 presented a surface fracture different from R1. Fe_3O_4 nanoparticles were clearly dispersed into the fracture surface of R_2 with nanosized nanoparticles that matched the nanosize provided by the Fe_3O_4 nanoparticles supplier. It is noted that some aggravated nanomaterials in both R_1 and R_2, as expected from nanomaterials that attracted each other by Van der Walls forces, and this finding matched the OM images. Interestingly, R_3 exhibited a strong impact when GO@Fe_3O_4 nanomaterials were combined, resulting in complex interactions and networks associated with notable changes in the fracture surfaces of the R_3sample. The intrinsic properties of GO@Fe_3O_4 nanomaterials could present a complex network of nanomaterials inside the MC matrix resulting from the interfacial interactions and combined effect of the alignment of the nanomaterials. This finding matched another reported finding [46]. The FESEM pictures exhibited clear correspondence to the XRD diffraction peaks, indicating the presence of diffraction patterns from both the GO flakes and Fe3O4 nanoparticles on the surface of R3. Furthermore, these nanomaterials exhibited a reduction in crystalline size compared to other samples. This can be attributed to the limitation of polymer crystallization growth, as detailed in Table 3.

Table 3 Summarizes the diffraction angle (2θ), interlayer displacement (d), crystallite size (D), typically FWHM (β), and Lattice Strain of samples

Samples	2θ, (˚)	d, (nm)	β, (°)	D, (nm)	Lattice Strain, [%]
MC	20.66	2.6	8.55	12.6	2.04
R1	20.55	4.68	2.35	37	6.36
R2	20.09	4.71	2.29	9.89	5.6
R3	21.06	4.50	1.12	5.63	2.7

Optical properties

Optical absorption of the samples was recorded in the range of 200–1100 cm^{-1}, represented in Fig. 5. The samples showed transition absorption peaks in the ultraviolet range at 200 nm. At 200 nm, MC hydrogel polymer revealed a π-π* plasmonic transition of about 2.8 related to the stacking vibration of C = C at 1650 cm^{-1} or the covalent bonding C–H and C–O. Loading GO into the hydrogel MC revealed a noticeable improvement in absorption from 2.8 of MC to 3.05 of MC/GO nanocomposites R_1at 200 nm. Absorption b = peaks increased to 3.2 after being replaced with GO with Fe_3O_4. It is worth noting that the result of GO@Fe_3O_4 in the scattering and absorption of light resulting from nanocomposite decreases the optical transparency of the samples up to 3.5, around 21%, which is the best result at higher energy. This proves that (GO NMS and Fe_3O_4) are evenly distributed throughout the polymer (MC). Large molecular chains strongly interact on surfaces and are accountable for the properties of the Fe_3O_4 polymer directly and GO.

Moreover, the absorption behavior was reduced and steady at the higher wavelength from 300 to 1100 nm. The contribution of nanomaterials was also clear in increasing the absorption in this area. For instance, samples' absorption increased from 0.04 of MC to 0.23 for R1, 0.42 for R2, and 1.09 for R3 at 700 nm, pointed around the middle of the wavenumber range. When the name or correlation contributes, it refers to the interface bonding between component matrices. The contributor electrons were a high conduction band excitation of the energy by attractive of known energy photon. The donor electrons could raise the energy level from low to high, so the outcomes presented strong photon absorption by the samples in the ultraviolet region.

The optical transmittance (T) spectrum of the polymer (MC) and nanocomposites was calculated using Eq. (4) [78], where (A) means the absorbance .

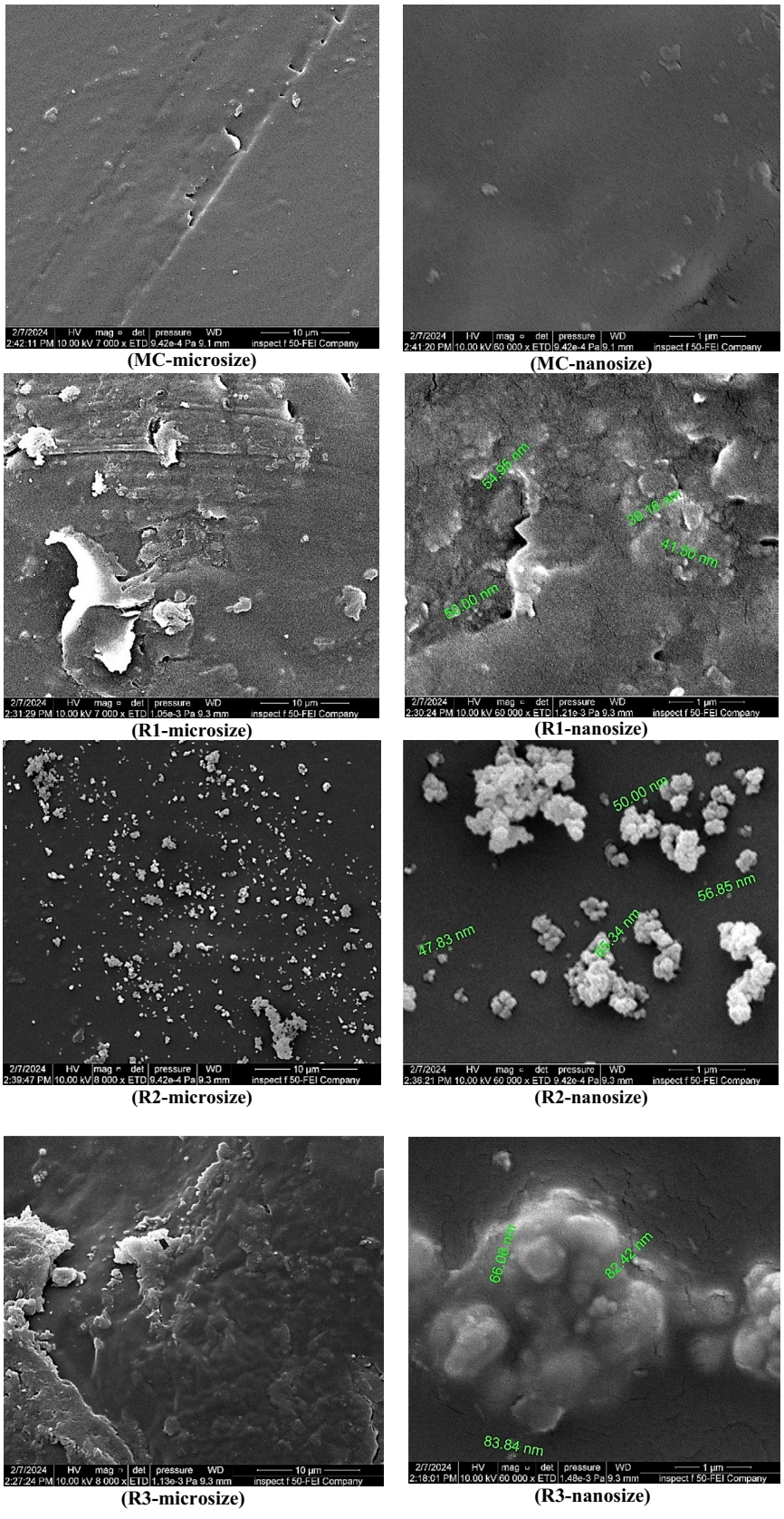

Fig. 4 FESEM images of samples (left side-microsize) and (right side-nanosize)

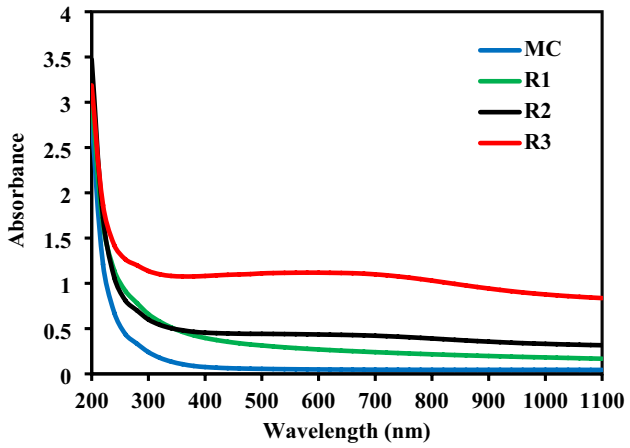

Fig. 5 The absorbance with wavenumber for the samples

$$A = -\log 10T \tag{4}$$

The MC film and nanocomposites are known to be highly absorbent near the leading absorption edge as exposed to the absorption coefficient (α), which is calculated by Eq. (5) [79].

$$\alpha = 2.303^{A}/_{t} \tag{5}$$

(t) means the thickness of the sample. The absorption coefficient for the samples is exposed in Fig. 6. It is noted that the absorption coefficient improves for samples with the contribution of Fe_3O_4 or GO NMS. R1 and R2 presented approximately the same behavior, whereas the combination of both nanomaterials in the hydrogel MC indicates an increase in the charge carrier in the nanocomposites associated with a significant increase in the r compared with other samples. Generally, the absorption coefficient values for all samples are enhanced with the growth of the energies. As a result, there is a small opportunity for electron transfer during the rise in the height of the incident photon, as shown in Fig. 6.

The energy that translates into high energy potential electron transfer, as the energy of incident photons, is sufficient to interact with atoms and is linked with the results of relevant investigations or samples. The energy gap is considered by Eq. (6) [80].

$$\alpha h\upsilon = B\left(h_{u-E_g}\right)^{r} \tag{6}$$

B, h_υ, and E_g are a constant and photon energy, as well as the optical energy gap, respectively, and r = 1/2 and 1/3 to allow and forbid indirect transitions. Figures 7 and 8 revealed the allowed and forbidden indirect transition optical band gap of the hydrogel MC polymer and its nanocomposites, respectively. It was considered by

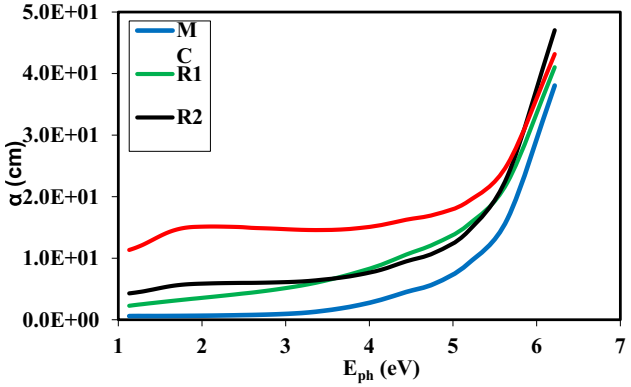

Fig. 6 The absorption coefficient of samples with the E_{ph}

plotting the intersection of the stable linear part; a direct line was drawn from the more significant part of the curve in Figs. 7 and 8 to look at the energy gap. The allowed and forbidden indirect transition optical band gap of hydrogel MC polymer revealed 4.79 and 4.05 electron volts, respectively. The results showed a slight decrease to 4.4 and 4.2, and 3.6 and 3.4 eV after loading GO nanosheets and Fe_3O_4. Interestingly, GO@Fe_3O_4 loading into MC resulted in additional redaction to 4.0 and 3.05 eV, as presented in Table 4.

This can be related to the modification of the polymer by loading nanomaterials, as the mechanisms can determine the levels between the valences with it, and in light of this. Under the situations, the electron moves from the valence band to the positioning levels and engages in optoelectronic devices, which agreed with other results (Table 4) [81].

The extinction coefficient (k) of the samples was considered from relationships (7) whereas, refractive index (n) are considered by (8) [82] and the results were revealed in Figs. 9 and 10, respectively.

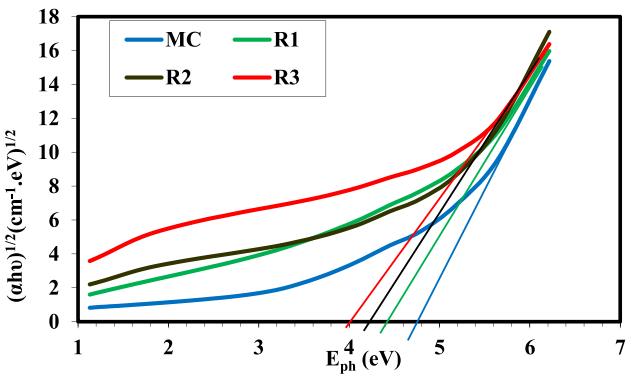

Fig. 7 The optical energy band gap $(\alpha h\nu)^{½}$ of allowed indirect transition for samples versus E_{ph}

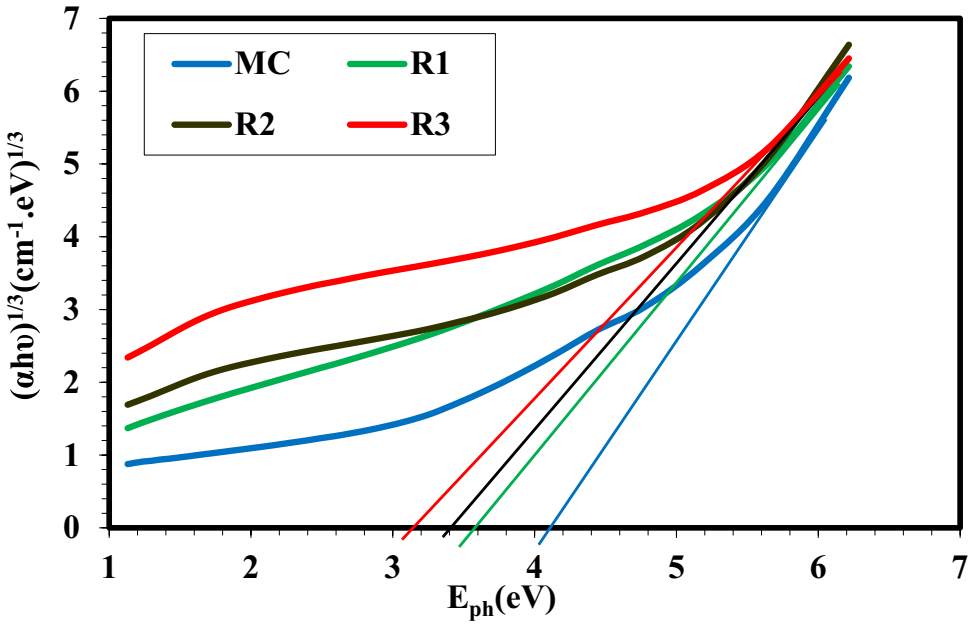

Fig. 8 The energy band gap $(\alpha h\nu)$ is $^{1/3}$ of the forbidden indirect transition for samples versus E_{ph}

Table 4 Indirect energy gap for samples

Samples	Allowed (eV)	Forbidden (eV)
MC	4.79	4.05
R_1	4.4	3.6
R_2	4.2	3.4
R_3	4.0	3.05

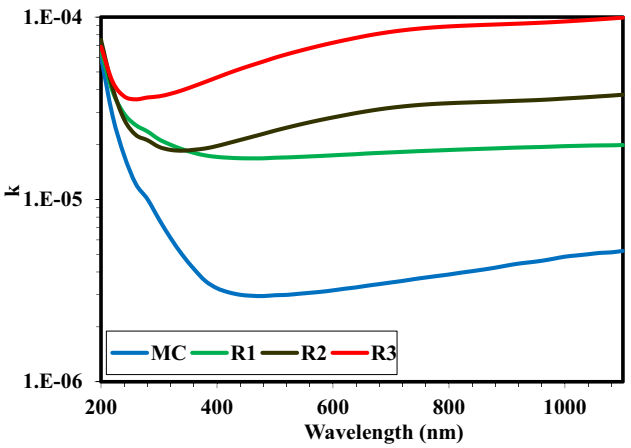

Fig. 9 K with wavelength for samples

$$k = \alpha\lambda/4\pi \tag{7}$$

λ is the wavelength, and the n is given by [83].

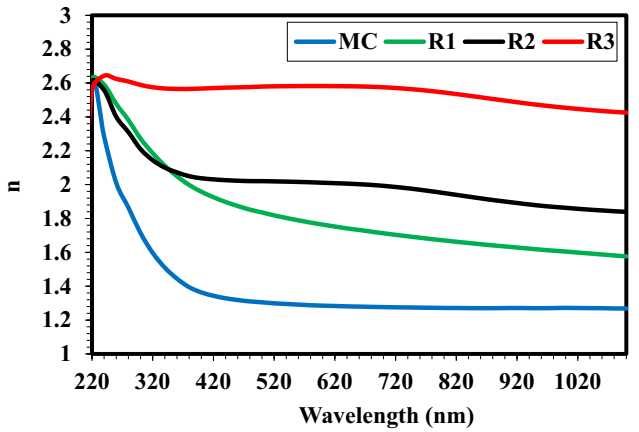

Fig. 10 n with wavelength for samples

$$n = \frac{1+\sqrt{R}}{1-\sqrt{R}} \tag{8}$$

R means reflectance. It was found that the k and the n increase with an increased contribution of GO, Fe_3O_4, and GO@Fe_3O_4 nanomaterials due to the difference in the value of (n) due to the structural change criterion, as shown in Figs. 9 and 10, respectively. Interestingly, the best result significantly increased with the contribution of both GO@Fe_3O_4 compared with other samples. This behavior could relate to an increase in the incident light absorption [84].

From the optical properties, new energy stages could be generated after the contribution of nanoparticles into the

host material within the band gap, such as states that either donate or accept states. These states can be stimulated by photons with longer wavelengths (lower energy), causing the absorption edge to move towards red-shifting (lower energies). Nanoparticles can alter the nearby dielectric conditions of the host substance [85]. This phenomenon can influence the polarisation of the material and subsequently impact the energies of the electronic transitions. As a result, there is a noticeable shift towards longer wavelengths, commonly referred to as a red shift, in the absorption edge [86].

The results of optical properties create possibilities for utilization in optoelectronic, solar cell, and optical sensors, as well as protection and filter applications.

The ideal wound sample is antibacterial since it is heavily contaminated with microorganisms. Consequently, investigations were conducted on the antibacterial activity of nanomembranes. The agar diffusion process was used well to evaluate the MC, and it is a nanocomposite. MC, GO, Fe_3O_4, GO@ Fe_3O_4, and nanocomposites were examined agonist the *S. aureus*, a gram-positive and *Pseudomonas aeruginosa,* a gram-negative bacterium, as presented in Figs. 11 and 12,

In Figs. 13 and 14, MC showed both bacteria's relatively weak inhibition zone. In contrast, GO showed an excellent ability up to 17 mm to kill both bacteria, whereas Fe_3O_4 exposed a better inhibition zone that improved up to 22 and 23, respectively. Interestingly, GO@ Fe_3O_4 revealed the best result of killing both bacteria up to 26 and 25 mm, respectively. R1, R2, and R3 were exposed to low relative results that matched MC results, as shown in Figs. 13 and 14. This could relate to the nanomaterials in this test, which MC totally covered due to the hydrogel nature that assisted this result in comparison to the nanomaterials used where the nanoparticles assist in the reactive oxygen generation, species-oxidative, and stress from reaction oxygen radicals (ROS). Where radicals, including superoxide dismutase, hydroxyl radicals (–OH), and (2–0) radicals (H_2O_2). These are involved in the oxygen radical's reaction, damaging the DNA and proteins of bacteria [87, 88]. This discovery is exciting for Bio-sensors and bacterial antimicrobials. The inhibition zone results presented promising samples, making them interesting biosensors, bacterial disinfectants, and other biomedical applications.

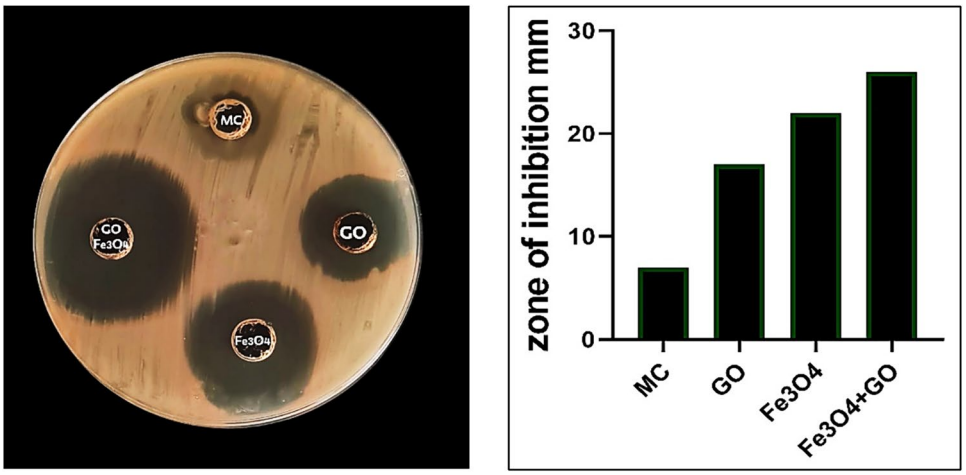

Fig. 11 MC, GO, Fe_3O_4, and Fe_3O_4@GO antibacterial activity against *S. aureus*

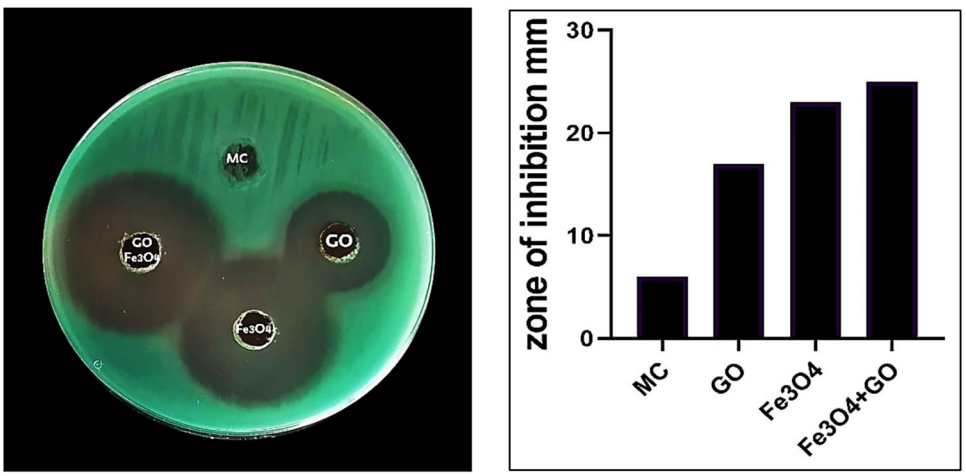

Fig. 12 MC, GO, Fe_3O_4, and Fe_3O_4 + GO antibacterial activity against *Pseudomonas aeruginosa*

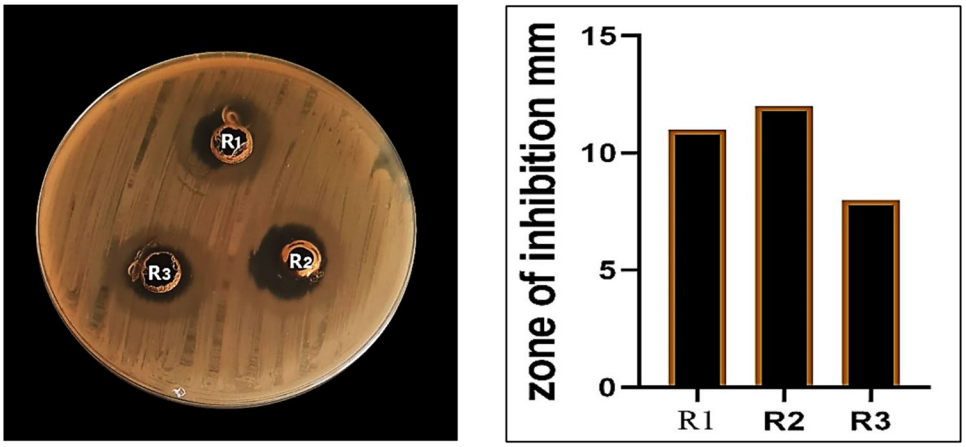

Fig. 13 R_1, R_2, and R_3 antibacterial activity against *S. aureus*

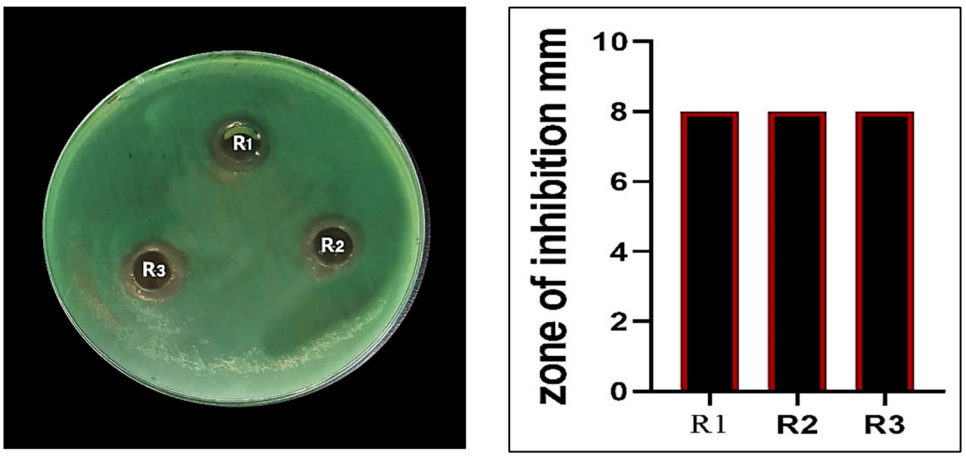

Fig. 14 R1, R2, and R3 antibacterial activity against *Pseudomonas aeruginosa*

Conclusion

The investigation successfully provided a fantastic comparison of the impact of two nanomaterials and their new nanocomposites. The Fe_3O_4 and synthesis GO were applied to fabricate new hydrolysis methylcellulose polymer MC nanocomposites. FTIR presented strong interactions among the components in the matrix. FESEM images showed a homogeneous surface and good dispersion of (GO and Fe_3O_4) In the polymer matrix, and smooth surfaces were clearly presented. As the concentration of nanoparticles increases with an increase in the concentration of additives (GO and Fe_3O_4), absorption increases without a significant impact on the transparency of the nanocomposites. The absorption behavior was improved by up to 21% after incorporating hybrid nanomaterials at 200 nm. Moreover, the energy gap in the indirect transfer is significantly reduced from 4.79 to 4.0 eV for the allowed indirect transitions and 4.05 to 3.05 eV and forbidden indirect transitions, which opens the opportunity for use in optoelectronic applications. The results of the antibacterial application of the composite compounds (Fe_3O_4@GO) showed notable improvement from 6 mm up to 26 and 25 mm of nanomaterials and to area where Staphylococcus aureus and Escherichia coli are located, respectively, prevented the increase. Used for objects with high antibacterial activity, it indicates that the work combines nanotechnology and biology to obtain new antimicrobials for medical applications. These results showed promising nanomaterials for optoelectronic devices, biosensors, bacterial disinfectants, and other applications.

Acknowledgements The authors thank the University of Sheffield, the UK, and the University of Babylon, Iraq, for their support.

Author contributions Rafah Mahdi Ahmed: Did the experimental work, investigated and analyzed the results, and wrote the draft. Ehssan Al-Bermany: Supervises the project's design and administration, reviews and editing, investigation, and resources.

Data availability The data are available in the manuscript.

References

1. Q. Wang, Y. Zhang, Y. Ma et al., Nano-crosslinked dynamic hydrogels for biomedical applications. Mater. Today Bio. **20**, 100640 (2023). https://doi.org/10.1016/j.mtbio.2023.100640
2. Z. Gan, X. Qin, H. Liu et al., Recent advances in defined hydrogels in organoid research. Bioact. Mater. **28**, 386–401 (2023). https://doi.org/10.1016/j.bioactmat.2023.06.004
3. K. Abdali, B.H. Rabee, E. Al-Bermany et al., Effect of doping Sb_2O_3 NPs on morphological, mechanical, and dielectric properties of PVA/PVP blend film for electromechanical applications. NANO **18**, 2350011 (2023). https://doi.org/10.1142/S179329202350011X
4. B. Mi, L. Chen, Y. Xiong et al., Osteoblast/osteoclast and immune cocktail therapy of an exosome/drug delivery multifunctional hydrogel accelerates fracture repair. ACS Nano **16**, 771–782 (2022). https://doi.org/10.1021/acsnano.1c08284
5. N.H. Thang, T.B. Chien, D.X. Cuong, Polymer-based hydrogels applied in drug delivery: an overview. Gels **9**, 1–38 (2023). https://doi.org/10.3390/gels9070523
6. A. Ayala-Ham, J. López-Gutierrez, M. Bermúdez et al., Hydrogel-based scaffolds in oral tissue engineering. Front. Mater. **8**, 1–26 (2021). https://doi.org/10.3389/fmats.2021.708945
7. G. Fang, X. Yang, Q. Wang et al., Hydrogels-based ophthalmic drug delivery systems for treatment of ocular diseases. Mater. Sci. Eng. C **127**, 112212 (2021). https://doi.org/10.1016/j.msec.2021.112212
8. S.A. Jasim, H.A.J. Banimuslem, F.H. Alsultany et al., Ammonia and nitrogen dioxide detection using ZnO/CNT nanocomposite synthesized by sol–gel technique. J. Sol-Gel Sci. Technol. **108**, 734–741 (2023). https://doi.org/10.1007/s10971-023-06190-y
9. A.N. Al-Jamal, K.H. Abbass, et al., *Silver NPs reinforced the structural and mechanical properties of PVA-PAAm-PEG nanocomposites*. In: AIP Conference Proceedings. (AIP Publishing LLC 2023), p. 030005
10. N.A. Peppas, R. Langer, New challenges in biomaterials. Science **263**, 1715–1720 (1994). https://doi.org/10.1126/science.8134835
11. E. Schelar, J. Liu, 25th Anniversary article: rational design and applications of hydrogels in regenerative medicine. Bone **23**, 1–7 (2008). https://doi.org/10.1002/adma.201303233.25th
12. E. Caló, V.V. Khutoryanskiy, Biomedical applications of hydrogels: a review of patents and commercial products. Eur. Polymer J. **65**, 252–267 (2015). https://doi.org/10.1016/j.eurpolymj.2014.11.024
13. R. Moreira, F. Chenlo, C. Silva, M.D. Torres, Rheological behaviour of aqueous methylcellulose systems: effect of concentration, temperature and presence of tragacanth. LWT **84**, 764–770 (2017). https://doi.org/10.1016/j.lwt.2017.06.050
14. H.S. Ragab, M.F.H. Abd El-Kader, Optical and thermal studies of starch/methylcellulose blends. Phys. Scr. **87**, 025602 (2013). https://doi.org/10.1088/0031-8949/87/02/025602
15. M.M. Pakulska, K. Vulic, R.Y. Tam, M.S. Shoichet, Hybrid crosslinked methylcellulose hydrogel: a predictable and tunable platform for local drug delivery. Adv. Mater. **27**, 5002–5008 (2015). https://doi.org/10.1002/adma.201502767
16. Y. Wang, L. Yu, Q. Sun, F. Xie, Hydroxypropyl methylcellulose and hydroxypropyl starch: rheological and gelation effects on the phase structure of their mixed hydrocolloid system. Food Hydrocoll. **115**, 106598 (2021). https://doi.org/10.1016/j.foodhyd.2021.106598
17. A. Najm Obaid, E. Al-Bermany, Impact of graphene nanosheets on adhesion and corrosion performance of reinforced polyurethane coating for aerospace aluminium alloy 2024–T3. Int. J. Adhes. Adhes. **132**, 103695 (2024). https://doi.org/10.1016/j.ijadhadh.2024.103695
18. L.S. Alqarni, A.M. Alghamdi, N.Y. Elamin, A. Rajeh, Enhancing the optical, electrical, dielectric properties and antimicrobial activity of chitosan/gelatin incorporated with Co-doped ZnO nanoparticles: nanocomposites for use in energy storage and food packaging. J. Mol. Struct. **1297**, 137011 (2024)
19. E. Al-Bermany, B. Chen, Effect of the functional groups of polymers on their adsorption behavior on graphene oxide nanosheets. Macromol. Chem. Phys. **224**, 2300101 (2023). https://doi.org/10.1002/macp.202300101
20. H.A. Mohammed, Optical fiber sensors coated with GO/PANI nanocomposite integrating a microcontroller-based acquisition and processing system. J. Opt. (2024). https://doi.org/10.1007/s12596-024-01712-5
21. A. Memic, H.A. Alhadrami, M.A. Hussain et al., Hydrogels 2.0: improved properties with nanomaterial composites for biomedical applications. Biomed. Mater. (Bristol) **11**, 014104 (2015). https://doi.org/10.1088/1748-6041/11/1/014104
22. E.M. Alharbi, A. Rajeh, Tailoring the structural, optical, dielectric, and electrical properties of PEO/PVA blend using graphene nanoplates for energy storage devices. J. Mater. Sci. Mater. Electron. **33**, 22196–22207 (2022). https://doi.org/10.1007/s10854-022-08999-9
23. M.T. Hussein, F.A. Hasan, E.K. Hassan, Studying the responsivity and detectivity of GO/PSi/n-Si photo detector via drop casting technique. J. Opt. **53**, 2161–2167 (2024). https://doi.org/10.1007/s12596-023-01355-y
24. A.K. Al-shammari, E. Al-Bermany, Polymer functional group impact on the thermo-mechanical properties of polyacrylic acid, polyacrylic amide- poly (vinyl alcohol) nanocomposites reinforced by graphene oxide nanosheets. J. Polym. Res. **29**, 351 (2022). https://doi.org/10.1007/s10965-022-03210-3
25. A.K. Al-shammari, E. Al-Bermany, New fabricated (PAA-PVA/GO) and (PAAm-PVA/GO) nanocomposites: functional groups and graphene nanosheets effect on the morphology and mechanical properties. J. Phys. Conf. Ser. **1973**, 012165 (2021). https://doi.org/10.1088/1742-6596/1973/1/012165
26. R.A. Ghazi, K.H. Al-Mayalee, E. Al-Bermany et al., Impact of polymer molecular weights and graphene nanosheets on fabricated PVA-PEG/GO nanocomposites: morphology, sorption behavior and shielding application. AIMS Mater. Sci. **9**, 584–603 (2022). https://doi.org/10.3934/matersci.2022035
27. N.R. Aldulaimi, E. Al-Bermany, New fabricated UHMWPEO-PVA hybrid nanocomposites reinforced by GO nanosheets: structure and DC electrical behaviour. J. Phys. Conf. Ser. **1973**, 012164 (2021). https://doi.org/10.1088/1742-6596/1973/1/012164
28. M.A. Kadhim, E. Al-Bermany, Enhance the electrical properties of the novel fabricated pmma-pva/ graphene based nanocomposites. J. Green Eng. **10**, 3465–3483 (2020)
29. A.M. Aboraia, I.S. Yahia, M. Saad et al., Exploration of the structural rGO thin films and their optical characteristics for optoelectronic device applications. J. Opt. (2024). https://doi.org/10.1007/s12596-024-02092-6
30. M.S. Jabir, U.M. Nayef, W.K. Abdulkadhim et al., Fe_3O_4 nanoparticles capped with PEG induce apoptosis in breast cancer AMJ13 cells via mitochondrial damage and reduction of NF-κB translocation. J. Inorg. Organomet. Polym. Mater. **31**, 1241–1259 (2021). https://doi.org/10.1007/s10904-020-01791-4
31. A. Ullah Khan, L. Chen, G. Ge, Recent development for biomedical applications of magnetic nanoparticles. Inorg. Chem. Commun. **134**, 108995 (2021). https://doi.org/10.1016/j.inoche.2021.108995
32. H.M. Alghamdi, M.M. Abutalib, A. Rajeh et al., Effect of the Fe_2O_3/TiO_2 nanoparticles on the structural, mechanical, electrical properties and antibacterial activity of the biodegradable chitosan/polyvinyl alcohol blend for food packaging. J. Polym. Environ. **30**, 3865–3874 (2022). https://doi.org/10.1007/s10924-022-02478-2

33. Y.T. Prabhu, K.V. Rao, B.S. Kumari et al., Synthesis of Fe_3O_4 nanoparticles and its antibacterial application. Int. Nano Lett. **5**, 85–92 (2015). https://doi.org/10.1007/s40089-015-0141-z
34. L.S. Arias, J.P. Pessan, A.P.M. Vieira et al., Iron oxide nanoparticles for biomedical applications: a perspective on synthesis, drugs, antimicrobial activity, and toxicity. Antibiotics **7**, 46 (2018). https://doi.org/10.3390/antibiotics7020046
35. M.D. Nguyen, H.-V. Tran, S. Xu, T.R. Lee, Fe_3O_4 nanoparticles: structures, synthesis, magnetic properties, surface functionalization, and emerging applications. Appl. Sci. **11**, 11301 (2021). https://doi.org/10.3390/app112311301
36. N.Y. Elamin, A. Modwi, W. Abd El-Fattah, A. Rajeh, Synthesis and structural of Fe_3O_4 magnetic nanoparticles and its effect on the structural optical, and magnetic properties of novel Poly(methyl methacrylate)/ Polyaniline composite for electromagnetic and optical applications. Opt. Mater. **135**, 113323 (2023)
37. E. Al-Bermany, A.T. Mekhalif, H.A. Banimuslem et al., Effect of green synthesis bimetallic Ag@SiO_2 core–shell nanoparticles on absorption behavior and electrical properties of PVA-PEO nanocomposites for optoelectronic applications. SILICON **15**, 4095–4107 (2023). https://doi.org/10.1007/s12633-023-02332-7
38. X. Yang, X. Zhang, Y. Ma et al., Superparamagnetic graphene oxide–Fe_3O_4 nanoparticles hybrid for controlled targeted drug carriers. J. Mater. Chem. **19**, 2710 (2009). https://doi.org/10.1039/b821416f
39. A.I. Alawi, E. Al-Bermany, R.S. Alnayli et al., Impact of SiO_2–GO hybrid nanomaterials on opto-electronic behavior for novel glass quinary (PAAm–PVP–PVA/SiO_2–GO) hybrid nanocomposite for antibacterial activity and shielding applications. Opt. Quant. Electron. **56**, 429 (2024). https://doi.org/10.1007/s11082-023-06070-3
40. É.C. de Oliveira, B.F. da Silva, P.F. Schopf et al., In vitro and in vivo safety profile assessment of graphene oxide decorated with different concentrations of magnetite. J. Nanopart. Res. **24**, 1–17 (2022). https://doi.org/10.1007/s11051-022-05529-w
41. N. Işıklan, N.A. Hussien, M. Türk, Hydroxypropyl cellulose functionalized magnetite graphene oxide nanobiocomposite for chemo/photothermal therapy. Colloids Surf A Physicochem Eng Asp **656**, 2–3 (2023). https://doi.org/10.1016/j.colsurfa.2022.130322
42. S. Yin, T. Zhang, Y. Yu et al., Study on the preparation and optical properties of graphene oxide@Fe_3O_4 two-dimensional magnetically oriented nanocomposites. Materials **16**, 476 (2023). https://doi.org/10.3390/ma16020476
43. G. Wang, G. Chen, Z. Wei et al., Multifunctional Fe_3O_4/graphene oxide nanocomposites for magnetic resonance imaging and drug delivery. Mater. Chem. Phys. **141**, 997–1004 (2013). https://doi.org/10.1016/j.matchemphys.2013.06.054
44. F.H. Dawood, N.S. Ahmed, F.A.-H. Mutlak, A novel approach to improve laser resonance via multilayer nano particles (Ag- GO -TiO_2) synthesized by pulsed laser deposition. J. Opt. (2024). https://doi.org/10.1007/s12596-024-01870-6
45. A. Atta, M.M. Abdelhamied, A.M. Abdelreheem, M.R. Berber, Flexible methyl cellulose/polyaniline/silver composite films with enhanced linear and nonlinear optical properties. Polymers **13**, 1–16 (2021). https://doi.org/10.3390/polym13081225
46. E. Sohouli, E.M. Khosrowshahi, P. Radi et al., Electrochemical sensor based on modified methylcellulose by graphene oxide and Fe_3O_4 nanoparticles: application in the analysis of uric acid content in urine. J. Electroanal. Chem. **877**, 114503 (2020). https://doi.org/10.1016/j.jelechem.2020.114503
47. M.A. Salam, F.H. Alsultany, E. Al-Bermany et al., Impact of graphene oxide nanosheets and polymethyl methacrylate on nano/hybrid-based restoration dental filler composites: ultrasound behavior and antibacterial activity. J. Ultrasound (2024). https://doi.org/10.1007/s40477-023-00855-8
48. H. Alhussain, A.M. Alghamdi, N.Y. Elamin, A. Rajeh, Recent progress in enhanced optical, mechanical, thermal properties, and antibacterial activity of the chitosan/polyvinylalcohol/Co_3O_4 nanocomposites for optoelectronics and biological applications. J. Polym. Environ. (2024). https://doi.org/10.1007/s10924-024-03191-y
49. S.M. Imani, L. Ladouceur, T. Marshall et al., Antimicrobial nanomaterials and coatings: current mechanisms and future perspectives to control the spread of viruses including SARS-CoV-2. ACS Nano **14**, 12341–12369 (2020). https://doi.org/10.1021/acsnano.0c05937
50. S.A. Jabbar, S.M. Khalil, A.R. Abdulridha et al., Dielectric, AC conductivity and optical characterizations of (PVA-PEG) doped SrO hybrid nanocomposites. Key Eng. Mater. **936**, 83–92 (2022). https://doi.org/10.4028/p-41a757
51. E. Hemmati, S. Soleimani-Amiri, M. Kurdtabar, A CMC- g -poly(AA- co -AMPS)/Fe3O4 hydrogel nanocomposite as a novel biopolymer-based catalyst in the synthesis of 1,4-dihydropyridines. RSC Adv. **13**, 16567–16583 (2023). https://doi.org/10.1039/D3RA01389H
52. F.S. Hashim, S.A. Jabbar, E. Al-Bermany, K. Abdali, Effect of inclusion ZnO-Co_3O_4 nanoparticles on the microstructural and optical properties of PVA-CMC polymeric blend for biomedical, UV shielding, and nuclear radiation shielding applications. Plasmonics (2024). https://doi.org/10.1007/s11468-024-02379-1
53. R.A.K. Al-Refai'a, K. Abdali, E. Al-Bermany, Some chloroquine derivatives for promising new antifungal drugs and absorption behavior. Int. J. Nanosci. (2023). https://doi.org/10.1142/S0219581X23500849
54. A.K. Hassan, H. Hamidinezhad, E. Al-Bermany, Antibacterial activity and optical behavior for restoration of micro and nano dental fillers using functional graphene nanosheets with polymethyl methacrylate. Nano Biomed. Eng. (2024). https://doi.org/10.26599/NBE.2024.9290075
55. H. Li, Q. Chen, J. Zhao, K. Urmila, Enhancing the antimicrobial activity of natural extraction using the synthetic ultrasmall metal nanoparticles. Sci. Rep. **5**, 11033 (2015). https://doi.org/10.1038/srep11033
56. I. Armentano, C.R. Arciola, E. Fortunati et al., The interaction of bacteria with engineered nanostructured polymeric materials: a review. Scientific World J. (2014). https://doi.org/10.1155/2014/410423
57. W. Gao, S. Thamphiwatana, P. Angsantikul, L. Zhang, Nanoparticle approaches against bacterial infections. Wiley Interdiscip. Rev.: Nanomed. Nanobiotechnol. **6**, 532–547 (2014)
58. B. Luan, T. Huynh, R. Zhou, Complete wetting of graphene by biological lipids. Nanoscale **8**, 5750–5754 (2016). https://doi.org/10.1039/c6nr00202a
59. A. Raghunath, E. Perumal, Metal oxide nanoparticles as antimicrobial agents: a promise for the future. Int. J. Antimicrob. Agents **49**, 137–152 (2017)
60. A.I. Alawi, E. Al-Bermany, Newly fabricated ternary PAAm-PVA-PVP blend polymer doped by SiO_2: absorption and dielectric characteristics for solar cell applications and antibacterial activity. SILICON **15**, 5773–5789 (2023). https://doi.org/10.1007/s12633-023-02477-5
61. M. Rajabi, K. Mahanpoor, O. Moradi, Preparation of PMMA/GO and PMMA/GO-Fe_3O_4 nanocomposites for malachite green dye adsorption: kinetic and thermodynamic studies. Compos. B Eng. **167**, 544–555 (2019). https://doi.org/10.1016/j.compositesb.2019.03.030
62. A.N. Obaid, E. Al-Bermany, Performance of functionalized graphene oxide to improve anti-corrosion of epoxy coating on 2024–T3 aluminium alloy. Mater. Chem. Phys. **305**, 127849 (2023). https://doi.org/10.1016/j.matchemphys.2023.127849
63. C. Donga, S.B. Mishra, L.N. Ndlovu et al., Magnetic magnetite-graphene oxide (Fe_3O_4-GO) nanocomposites for removal of

dyes from aqueous solution. J. Inorg. Organomet. Polym. Mater. (2024). https://doi.org/10.1007/s10904-024-03077-5
64. A.A. Fadhl Abodood, K. Abdali, A.O. Mousa Al-Ogaili et al., Effect of molar concentration and solvent type on linear and NLO properties of aurintricarboxylic (ATA) organic dye for image sensor and optical limiter applications. Int. J. Nanosci. **22**, 22–23 (2023). https://doi.org/10.1142/S0219581X2350014X
65. A.N. Tuama, E. Al-Bermany, R.S. Alnayli et al., A critical review of the evaluation of Sio_2-incorporated Tio_2 nanocomposite for photocatalytic activity. SILICON (2024). https://doi.org/10.1007/s12633-024-02870-8
66. K. Abdali, E. Al-Bermany, K.H. Abass et al., Impact the silver nanoparticles on properties of new fabricated polyvinyl alcohol-polyacrylamide- polyacrylic acid nanocomposites films for optoelectronics and radiation pollution applications. J. Polym. Res. **30**, 138 (2023). https://doi.org/10.1007/s10965-023-03514-y
67. H.H. Bahjat, R.A. Ismail, G.M. Sulaiman, M.S. Jabir, Magnetic field-assisted laser ablation of titanium dioxide nanoparticles in water for anti-bacterial applications. J. Inorg. Organomet. Polym. Mater. **31**, 3649–3656 (2021). https://doi.org/10.1007/s10904-021-01973-8
68. K.S. Khashan, F.A. Abdulameer, M.S. Jabir et al., Anticancer activity and toxicity of carbon nanoparticles produced by pulsed laser ablation of graphite in water. Adv. Nat. Sci.: Nanosci. Nanotechnol. **11**, 035010 (2020). https://doi.org/10.1088/2043-6254/aba1de
69. G.S. Jaber, K.S. Khashan, M.J. Abbas, Study the antibacterial activity of zinc oxide nanoparticles synthesis by laser ablation in liquid. Mater. Today: Proc. **42**, 2668–2673 (2021). https://doi.org/10.1016/j.matpr.2020.12.646
70. M.A. Jihad, F.T.M. Noori, M.S. Jabir et al., Polyethylene glycol functionalized graphene oxide nanoparticles loaded with *Nigella sativa* extract: a smart antibacterial therapeutic drug delivery system. Molecules **26**, 3067 (2021). https://doi.org/10.3390/molecules26113067
71. M.K.A. Mohammed, M.R. Mohammad, M.S. Jabir, D.S. Ahmed, Functionalization, characterization, and antibacterial activity of single wall and multi wall carbon nanotubes. IOP Conf. Ser.: Mater. Sci. Eng. **757**, 012028 (2020). https://doi.org/10.1088/1757-899X/757/1/012028
72. S. Maleky, A. Asadipour, A. Nasiri et al., Tetracycline adsorption from aqueous media by magnetically separable Fe_3O_4@methylcellulose/APTMS: isotherm, kinetic and thermodynamic studies. J. Polym. Environ. **30**, 3351–3367 (2022). https://doi.org/10.1007/s10924-022-02428-y
73. R.A. Abdul-Nabi, E. Al-Bermany, Performers of Si_3N_4 concentrations on morphology and electrical behavior for new quinary fabrication PEO-CMC-PANI/GO@Si_3N_4 nanocomposites for electronic devise and gas sensor application. SILICON (2024). https://doi.org/10.1007/s12633-024-03092-8
74. S. Erogul, S.Z. Bas, M. Ozmen, S. Yildiz, A new electrochemical sensor based on Fe_3O_4 functionalized graphene oxide-gold nanoparticle composite film for simultaneous determination of catechol and hydroquinone. Electrochim. Acta **186**, 302–313 (2015). https://doi.org/10.1016/j.electacta.2015.10.174
75. G. Cao, Q. Zhang, C. Jeffrey Brinker, *Annual Review of Nano Research*, vol. 3 (World Scientific, Singapore, 2009)
76. M. Qiu, Y. Zhang, B. Wen, Facile synthesis of polyaniline nanostructures with effective electromagnetic interference shielding performance. J. Mater. Sci. Mater. Electron. **29**, 10437–10444 (2018). https://doi.org/10.1007/s10854-018-9100-6
77. A. Khorsand Zak, J. Esmaeilzadeh, A.M. Hashim, X-ray peak broadening and strain-driven preferred orientations of pure and Al-doped ZnO nanoparticles prepared by a green gelatin-based sol-gel method. J. Mol. Struct. **1303**, 137537 (2024). https://doi.org/10.1016/j.molstruc.2024.137537
78. P.B. Allen, Elementary solid state physics: principles and applications by M A. Omar. Am. J. Phys. **43**, 929–933 (1975). https://doi.org/10.1119/1.9980
79. M. Jothibas, C. Manoharan, S. Johnson Jeyakumar, P. Praveen, Study on structural and optical behaviors of In2O3 nanocrystals as potential candidate for optoelectronic devices. J. Mater. Sci. Mater. Electron. **26**, 9600–9606 (2015). https://doi.org/10.1007/s10854-015-3623-x
80. T. Abdel-Baset, M. Elzayat, S. Mahrous, Characterization and optical and dielectric properties of polyvinyl chloride/silica nanocomposites films. Int. J. Polym. Sci. **2016**, 1–13 (2016). https://doi.org/10.1155/2016/1707018
81. K. Abdali, K.H. Abass, E. Al-Bermany et al., Morphological, optical, electrical characterizations and anti- *Escherichia coli* bacterial efficiency (AECBE) of PVA/PAAm/PEO polymer blend doped with silver NPs. Nano Biomed. Eng. **14**, 114–122 (2022). https://doi.org/10.5101/nbe.v14i2.p114-122
82. R. Levinson, P. Berdahl, H. Akbari, Solar spectral optical properties of pigments - Part I: model for deriving scattering and absorption coefficients from transmittance and reflectance measurements. Sol. Energy Mater. Sol. Cells **89**, 319–349 (2005). https://doi.org/10.1016/j.solmat.2004.11.012
83. S. Agarwal, Y.K. Saraswat, V.K. Saraswat, Study of optical constants of ZnO dispersed PC/PMMA blend nanocomposites. Open Phys. J. **3**, 63–72 (2016). https://doi.org/10.2174/1874843001603010063
84. SS. Al-Abbas, R.A. Ghazi, E. Al-Bermany, et al., *Structure and absorption behaviour of PAAm-PVA-based nanocomposites reinforced using graphene*. In: AIP Conference Proceedings. (2023) p. 090056
85. A.A.A. Najm, S.M. Alshrefi, Z.L. Hadi et al., Synthesis of novel [CdO(75%)/VO2(20%)/SiC(4%):p-Si] heterojunction composite thin films decorated with chlorophyll using solvothermal-laser dual technique for solar cell applications. SILICON **2**, 1–4 (2024). https://doi.org/10.1007/s12633-024-02997-8
86. M.K. Omar, N.M. Ahmed, A.A.M. Alqanoo et al., Performance evaluation of aluminum nitride-decorated AgNWs-based transparent conductive electrodes deposited on flexible substrates. J. Mater. Sci. Mater. Electron. (2024). https://doi.org/10.1007/s10854-024-12211-5
87. S.S. Aljelawy, E. Al-Bermany, A.R. Abdulridha, Performance of graphene-functionalized nano chitosan in ternary polymeric nanocomposites for physical and biological applications. J. Polym. Res. **31**, 226 (2024). https://doi.org/10.1007/s10965-024-04064-7
88. S.A.J. Mohammed, R.M.S. Al-Haddad, B.K. Al-Rawi, NIR laser effect on cancer cell lines activity by using Fe_3O_4@Cu@SiO_2 core–shell nanoparticles. J. Opt. (2024). https://doi.org/10.1007/s12596-024-01676-6

Publisher's Note Springer Nature remains neutral with regard to jurisdictional claims in published maps and institutional affiliations.

Springer Nature or its licensor (e.g. a society or other partner) holds exclusive rights to this article under a publishing agreement with the author(s) or other rightsholder(s); author self-archiving of the accepted manuscript version of this article is solely governed by the terms of such publishing agreement and applicable law.